Airborne observations of regional variation in fluorescent aerosol across the United States

A. E. Perring[1,2], J. P. Schwarz[1,2], D. Baumgardner[3], M. T. Hernandez[4], D. V. Spracklen[5], C. L. Heald[6], R. S. Gao[1], G. Kok[3], G. R. McMeeking[3], J. B. McQuaid[5], and D. W. Fahey[1]

[1]NOAA Earth Systems Research Laboratory, Boulder, Colorado, USA, [2]Cooperative Institute for Research in Environmental Sciences, University of Colorado Boulder, Boulder, Colorado, USA, [3]Droplet Measurement Technologies, Boulder, Colorado, USA, [4]Department of Civil, Environmental, and Architectural Engineering, University of Colorado Boulder, Boulder, Colorado, USA, [5]School of Earth and Environment, University of Leeds, Leeds, UK, [6]Department of Civil and Environmental Engineering, Massachusetts Institute of Technology, Boston, Massachusetts, USA

Abstract Airborne observations of fluorescent aerosol were made aboard an airship during CloudLab, a series of flights that took place in September and October of 2013 and covered a wideband of longitude across the continental U.S. between Florida and California and between 28 and 37 N latitudes. Sampling occurred from near the surface to 1000 m above the ground. A Wideband Integrated Bioaerosol Sensor (WIBS-4) measured average concentrations of supermicron fluorescent particles aloft (1 μm to 10 μm), revealing number concentrations ranging from 2.1 ± 0.8 to $8.7 \pm 2.2 \times 10^4$ particles m^{-3} and representing up to 24% of total supermicron particle number. We observed distinct variations in size distributions and fluorescent characteristics in different regions, and attribute these to geographically diverse bioaerosol. Fluorescent aerosol detected in the east is largely consistent with mold spores observed in a laboratory setting, while a shift to larger sizes associated with different fluorescent patterns is observed in the west. Fluorescent bioaerosol loadings in the desert west were as high as those near the Gulf of Mexico, suggesting that bioaerosol is a substantial component of supermicron aerosol both in humid and arid environments. The observations are compared to model fungal and bacterial loading predictions, and good agreement in both particle size and concentrations is observed in the east. In the west, the model underestimated observed concentrations by a factor between 2 and 4 and the prescribed particle sizes are smaller than the observed fluorescent aerosol. A classification scheme for use with WIBS data is also presented.

1. Introduction

Primary biological aerosol particles (PBAPs, also denoted "bioaerosols") are directly emitted from the Earth's surface through a variety of mechanisms, in a wide range of sizes from tens of nanometers for viruses to hundreds of micrometers for plant fragments. A full description of the kinds of bioaerosol found in the atmosphere, as well as current techniques for their measurement, is available in the recent review by *Després et al.* [2012]. These particles are of growing interest for the atmospheric science community in large part due to their potential influence on cloud formation and precipitation. As discussed in more detail below, they may play important roles as both ice nuclei (IN) and giant cloud condensation nuclei (CCN), which could represent a significant feedback between ecosystems and meteorology.

PBAPs have been observed to heterogeneously nucleate ice at temperatures as high as −2°C in laboratory mixtures [*Diehl et al.,* 2002; *Iannone et al.,* 2011] and have been measured both in cloud ice residuals [*Pratt et al.,* 2009] and in precipitation [*Christner et al.,* 2008; *Hill et al.,* 2014; *Joly et al.,* 2013]. *Creamean et al.* [2013] recently reported a direct link between long-range transport of biological aerosol and precipitation in the Sierra Nevada. Recent modeling work indicates that PBAP may be responsible for nearly all immersion freezing at 480 hPa between 30°S and 30 N [*Spracklen and Heald*, 2014] and that oceanic PBAP emissions may be the primary source of IN over the remote ocean [*Burrows et al.,* 2013]. In addition to their potential role in direct heterogeneous ice nucleation, several studies have suggested that PBAP may also be responsible for initiating cascading secondary ice production [*Crawford et al.,* 2012; *Morris et al.,* 2014] that would amplify the impacts of bioaerosol on clouds, especially in regions of high emission.

PBAPs have been observed to be a significant fraction of supermicron aerosol in certain environments. Notably, in the Amazon, fluorescent particle loads (as a surrogate measure of PBAP) accounted for 24–40% of the total coarse-mode aerosol number [*Huffman et al.,* 2012; *Pöschl et al.,* 2010] and a wide range of contributions (from 5 to 30%) have been found during several studies in Europe [*Huffman et al.,* 2010; *Jaenicke et al.,* 2007; *Toprak and Schnaiter,* 2013]. As discussed by *Delort et al.* [2010] this indicates that PBAP may play a significant role in cloud formation and precipitation, especially if they serve as giant CCN capable of droplet formation at low supersaturations. Large CCN can have substantial impacts on cloud droplet size distributions and precipitation behavior. For example, *Konwar et al.* [2012] found that the presence of giant CCN lowered both the threshold droplet diameter and the altitude level at which warm rain was produced. As discussed in detail by *Morris et al.* [2014], if PBAP from either the terrestrial or marine environment constitute a considerable fraction of giant CCN or IN particles, then there may be several powerful feedbacks between ecological communities and meteorology.

Observational evidence regarding the global importance of PBAP, however, is sparse, especially in the vertical dimension. A few ground-based high-altitude studies have found distinct bacterial and fungal populations in the midtroposphere [*Bowers et al.,* 2012, 2009; *Smith et al.,* 2013], and high concentrations of bacteria were recently reported above a hurricane [*DeLeon-Rodriguez et al.,* 2013]. Additionally, two recent studies have reported fluorescent particle counts at high-altitude ground sites. *Gabey et al.* [2013] report fluorescent concentrations of up to $270 \, \mathrm{L}^{-1}$ at Puy de Dôme in France and *Hallar et al.* [2011] report evidence of PBAP attached to dust at Storm Peak in Colorado yet the geographic extent of the available measurements is inadequate for assessing regional and global effects of bioaerosol. Modeled emission rates of airborne bacteria and fungal (mold and mushroom) spores are primarily based on a relatively small set of surface data, and parameterizations vary widely [*Burrows et al.,* 2009b; *Heald and Spracklen,* 2009; *Hoose et al.,* 2010a; *Sesartic et al.,* 2013]. Further measurements of PBAP in a variety of environments and seasons are required to fully assess global concentrations and variability, and to evaluate theorized linkages between PBAP and cloud properties and precipitation.

Until recently, PBAPs have been counted following impaction onto a collection medium, or impingement into liquids. This is generally labor intensive and often involves long collection times in ambient sampling to obtain sufficient biomass for accurate counting or genetic profiling, precluding its application in high-speed aircraft sampling. Several instruments have been developed in recent years that quantify the autofluorescent properties of biological particles and thus allow in situ, single-particle detection of fluorescent PBAP (sometimes abbreviated FBAP in the literature) [*Huffman et al.,* 2010; *Kaye et al.,* 2005] facilitating real-time measurements of fluorescent PBAP concentrations.

Here we report observations of fluorescent aerosol, which we use as a proxy for fluorescent PBAP. For ease of discussion, fluorescent PBAP is used interchangeably with "fluorescent aerosol" in what follows although we recognize that the technique is less specific to biological material than are the more established impaction methods. The validity of using fluorescent particle concentrations as a proxy for PBAP is a topic of debate. There are potential artifacts from nonbiological fluorescent particles, uncertainty regarding the fraction of atmospheric PBAP that is fluorescent, and unknown impacts of atmospheric aging on the PBAP autofluorescence. Currently, there is inadequate information to reliably determine the representativeness of fluorescent particle observations for true atmospheric PBAP, and more research is warranted. The behavior of both known biological materials and potential interferents in the WIBS is discussed below as well as additional factors (such as particle size) that can be used to assess the likelihood that a given fluorescent particle is biological in origin.

The measurements discussed here were made aboard an airship that typically operated at 300 m above ground level with occasional excursions up to 1 km altitude. The campaign, covering a wide swath of longitude across the southern United States, allows for assessment of fluorescent PBAP concentrations and characteristics with an unprecedented geographic extent. A new categorization scheme is presented whereby fluorescent particles are classified as one of seven "types" based on their fluorescence behavior. Variations in concentration and number distribution of each type are analyzed in 10 different geographic regions sampled during the study, and the observed loadings are compared to simulated PBAP concentrations.
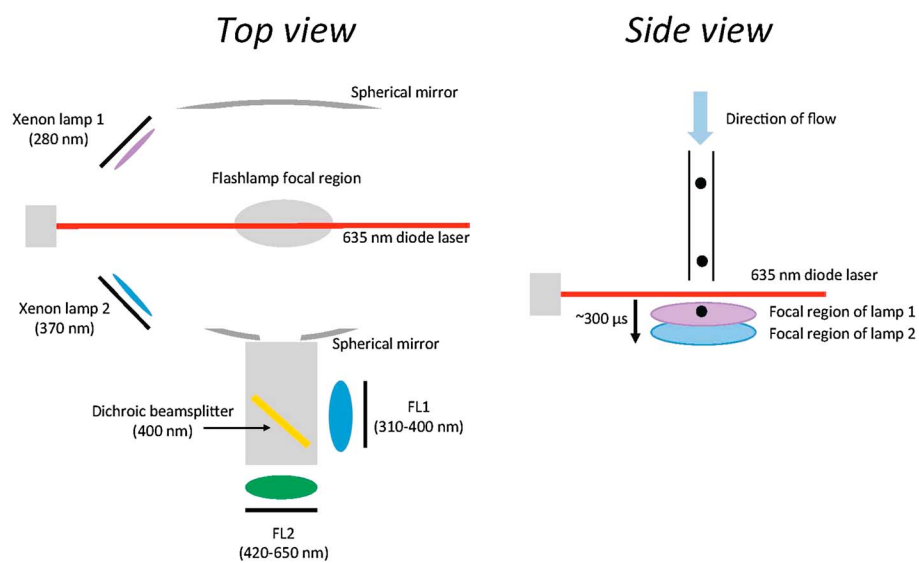
Figure 1. Schematic diagram of the WIBS detection cell as viewed from (left) above and the (right) side showing the orientation of the Xenon flash lamps, PMT detectors, red triggering laser, and spherical mirrors.

2. Methods

2.1. Instrumentation

2.1.1. The WIBS-4

Individual fluorescent particles were detected with a Wideband Integrated Bioaerosol Sensor (WIBS-4, Droplet Measurement Technologies, Inc., Boulder, Colorado), which has been described previously [*Gabey et al.,* 2010; *Kaye et al.,* 2005]. A schematic of the WIBS detection block is shown in Figure 1. Briefly, aerosol particles are drawn through a 635 nm continuous wave laser, and the resulting elastically scattered light is detected and used to count and size all incoming particles in the diameter size range ~0.8–14 μm in the present configuration. In what follows, we have limited our analysis to particles with optical size greater than 1 μm both for simplicity and to reduce uncertainty related to potential nonunitary detection efficiency near the limit of detection. The scatter signal sequentially triggers two Xenon flashlamps filtered to emit UV light at 280 nm and 370 nm wavelengths. Any fluorescence emitted by the particle due to these excitations is imaged onto two photomultiplier tubes (PMTs, Hamamatsu H10720-110), equipped with filters to detect light from 310 to 400 nm (the FL1 detector) and from 420 to 650 nm (the FL2 detector). This system provides three pieces of fluorescent information for each particle: (i) Channel A: emission recorded by the FL1 detector following excitation at 280 nm (also referred to as the FL1_280 channel in other work); (ii) Channel B: emission recorded by the FL2 detector following excitation at 280 nm (also referred to as the FL2_280 signal); and (iii) Channel C: emission recorded by the FL2 detector following excitation at 370 nm (also referred to as the FL2_370 signal).

Elastically scattered 370 nm excitation light saturates the FL1 channel, so it does not add additional information. The excitation and emission wavelength bands were chosen to roughly correspond to the excitation and emission of tryptophan (channel A) and the reduced form of nicotinamide adenine dinucleotide (abbreviated NADH, detected in channel C). These are two fluorophores that are ubiquitous in microbiological cells and plant tissues; however, many other biomolecules can also contribute fluorescence in these bandwidths. For an overview of possible fluorophores both biological and nonbiological, we refer the reader to an impressive series of laboratory experiments reported by *Pöhlker et al.* [2012]. The potential combinations of fluorescence signals detected by the WIBS are discussed in more detail in section 2.1.3.

The scattered laser light used for triggering, counting, and sizing is imaged on the FL2 detector, and the particle size range of detection is determined by the gain of this sensor. As configured here, the size range detected was 0.8 μm to 14 μm equivalent optical diameter, similar to that reported by *Healy et al.* [2012a]. This size range pertains only to detection by the instrument itself and not to additional limitations imposed by the airship inlet configuration, which are discussed in more detail below. The WIBS-4 stores the raw peak height

from the scattered laser light, which is used in conjunction with Mie theory to obtain an optical particle size. Note that the equivalent optical diameter can be very different from the physical diameter depending on particle morphology. The Mie theory calculations are in good agreement with data taken in the laboratory using a range of polystyrene latex spheres (PSLs) between 0.75 μm and 4 μm. The instrument used during the CloudLab project was calibrated in the laboratory using 2 μm green fluorescent PSLs (Fisher Scientific) before and after the mission and in the field on 29 September 2013.

Forward scattered laser light is imaged onto a quadrant photo detector (QPD) to calculate an asymmetry factor (AF), which provides information on particle morphology [*Healy et al.,* 2012b; *Toprak and Schnaiter,* 2013]. Unfortunately, the laser and QPD alignments in the present study were inadequate to extract useful AF values over the size range of interest. We therefore do not include the AF measurement in our analysis. The maximum flash rate of the Xenon lamps is approximately 125 Hz so not all particles passing through the cavity will be irradiated when particle concentrations are high. The instrument records both the number of particles that pass through the laser beam and the number of particles for which the lamps flash. Data presented here have been corrected to account for particles missed by the flashlamps. The correction applied to 1 min average data was typically less than 5%, and data were rejected if more than 20% of the particles were missed by the flashlamps.

Attribution of the fluorescence signals detected by the WIBS to specific types of PBAP is an active area of study. Individual fungal spores, which are typically between 2 and 20 μm in the environment, are expected to be a large fraction of atmospheric PBAP with estimated global emissions of between 28 and 186 Tg/yr [*Heald and Spracklen,* 2009; *Hoose et al.,* 2010a; *Jacobson and Streets,* 2009; *Sesartic and Dallafior,* 2011]. The ability of fluorescence spectroscopy instruments to detect fungal spores has recently been evaluated by several studies [*Healy et al.,* 2012b; *Huffman et al.,* 2010, 2012]. *Healy et al.* [2014] found good correlations between counts from a Sporewatch particle impactor and certain fluorescence channels in both the WIBS-4 and an Ultraviolet Aerosol Particle Sizer (UV-APS, TSI Incorporated, Shoreview, Minnesota) during ambient sampling in Ireland. Therefore, based on previous work, the WIBS is likely counting a substantial fraction of airborne spores in the present study as well as airborne hyphae and tissue fragments which are fungal in origin but are not spores.

Less is known about the ability of the WIBS to detect bacteria, which are predicted to be another important source of PBAP with global emissions estimated to be between 0.74 and 28.1 Tg/yr [*Burrows et al.,* 2009a; *Hoose et al.,* 2010a; *Jacobson and Streets,* 2009]. Emission spectra of several kinds of bacteria have been measured at a variety of excitation wavelengths [*Hill et al.,* 2009; *Pan et al.,* 2014b], as a function of particle size, illumination intensity, and fluorophore concentration [*Hill et al.,* 2001] and as a function of oxidation and humidity [*Pan et al.,* 2014a]. Bacteria typically have strong absorption features around 280 nm with emission occurring between 310 and 400 nm. Occasionally, they have weaker absorption and emission at longer wavelengths. Most individual bacterial cells are less than 2 μm, which means that a large fraction of them are likely too small to be discretely recognized by the WIBS-4 in its present configuration. *Toprak and Schnaiter* [2013], however, report near unit detection efficiency for *Pseudomonas syringae* in Channel A, and bacteria have been observed attached to dust particles that do fall within the WIBS size range [*Hallar et al.,* 2011] although the detection efficiency for WIBS measurements of bacteria-dust agglomerates is unknown. Therefore, the WIBS likely detects a fraction of airborne bacteria present in the sample stream and will likely recognize bacterial clusters and/or bacterial spores.

Pollen is another major contributor to PBAP with global emissions estimated to be 84.5 Tg/yr [*Jacobson and Streets,* 2009]. Several studies have investigated the detection of pollen using the WIBS [*Healy et al.,* 2012b; *O'Connor et al.,* 2014]. We note that many intact grains would be too large (> 10 μm) for transport to the WIBS in the present configuration; however, smaller grains or pollen fragments likely are sampled and would be detected by the WIBS.

There are several things to keep in mind with regard to WIBS-based measurements of fluorescent aerosol. First, it is important to note that the size determination of the WIBS is based exclusively on scattered laser light. Thus, the numbers presented here represent optical particle size, which can be substantially different from physical particle size, especially for nonspherical particles. Second, variations in particle orientation within the WIBS cavity may affect the optical size determination and/or the detected fluorescent intensity. This would yield variable results for identical particles passed through the instruments at different times

and increases the uncertainty in the measurement. Finally, as mentioned above there are a number of anthropogenic aromatic compounds that can have fluorescent signals in the bands used in the WIBS. A number of these compounds are explored in *Pöhlker et al.* [2012]. The WIBS particle count is not affected by background fluorescence resulting from gas phase species; however, these molecules may be attached to larger dust or soil particles which would contribute to the WIBS fluorescent particle count. Some evidence of anthropogenic interferences is observed in this work, and it is discussed in section 3.4 below. In general, if fluorescent particles appear with a modal size distribution peaking at a different size than does the bulk aerosol, it seems more likely that those particles are truly PBAP. It is harder to separate anthropogenic interferents from PBAP in the smaller size ranges (i.e., bacteria) where there is substantial overlap between background accumulation-mode aerosol and the biological particles of interest.

2.1.2. Fluorescent Threshold Determination

To obtain meaningful fluorescent particle counts from a WIBS, care is required in choosing the signal level above which a particle is considered to be fluorescent (within each channel of detection). The WIBS is designed to allow determination of this threshold by using the signal observed in the three fluorescence channels when the flashlamps are triggered automatically (at a frequency of ~2 Hz) without particles in the cavity. The threshold found in this "forced trigger" mode accounts for flashlamp light that leaks through the PMT filters. The signal strength in this background mode depends on the output power of the Xenon lamps, the filter transmission function, the detector gain, and any light from fluorescent materials deposited to the walls of the detection chamber [*Toprak and Schnaiter*, 2013]. Typically, the fluorescence threshold is calculated from forced trigger data only. *Gabey et al.* [2010], for example, classified particles as fluorescent if they produced signals 2.5 standard deviations above the mean of the forced trigger intensity for a given channel, while *Toprak and Schnaiter* [2013] classified them as fluorescent if the signals exceeded the 3 standard deviation level. The instrument is usually operated in forced trigger mode occasionally (daily to weekly), and *Toprak and Schnaiter* [2013] found very little variation in forced trigger measurements over the course of a yearlong measurement campaign under ambient conditions. In the present study, forced trigger data were collected on most days either before or after a flight. The calculated fluorescence thresholds, especially in the FL1_280 channel, exhibited larger variations than previously seen (up to 25% between subsequent forced trigger measurements). These variations are large enough to significantly change the number of particles identified as fluorescent. Hence, we determine the fluorescence threshold at higher time resolution than that afforded from the forced trigger data alone by analysis of nonfluorescent ambient particles sampled throughout our data set under normal operating conditions.

Occurrence histograms were made for each channel using signals from blocks of 10,000 events triggered by ambient particles, corresponding to collection times of between 10 min and 1 h depending on the ambient particle loadings. These histograms were then fit with a Gaussian-constrained probability distribution to include a subset of points spanning from before the peak of the histogram to when the frequency had fallen to 85% of its peak value. Histograms are used rather than means and fit to a subset of the data to account for the fact that the ambient particles of interest exhibit fluorescence and create a tail at the high end of the distribution that skews a simple arithmetic mean. An example histogram of the background fluorescence from the FL1_280 channel and the associated Gaussian fit is shown for ambient particles in Figure 2a. Shown for comparison is a histogram (and fit) of forced trigger data taken in the same channel just prior to the ambient histogram. Since the fits to the two histograms have very similar centers and widths, the fluorescence threshold values derived from forced trigger and ambient data are similar. Figure 2b shows the fluorescence threshold as a function of time over the course of the flight for the same forced trigger and ambient data used in Figure 2a. This agreement between forced trigger and temporally proximate ambient data was consistently observed throughout the sampling campaign. Typically, the background was highest and most variable early in the flight, decreasing to a more stable value over the first hour or so. While the variable background was primarily apparent in the FL1_280 channel, we have determined fluorescence thresholds equivalently for all three channels for consistency.

The agreement between forced trigger and ambient determinations of fluorescence thresholds is sufficient evidence that the presence of any nonfluorescent particles in the cavity has a negligible impact on the amount of flashlamp light reaching the detectors, a conclusion supported by laboratory measurements of known nonfluorescent polystyrene latex spheres. The fluorescence thresholds determined from the forced trigger mode and ambient particles, therefore, capture variations in flashlamp output power, detector gain,
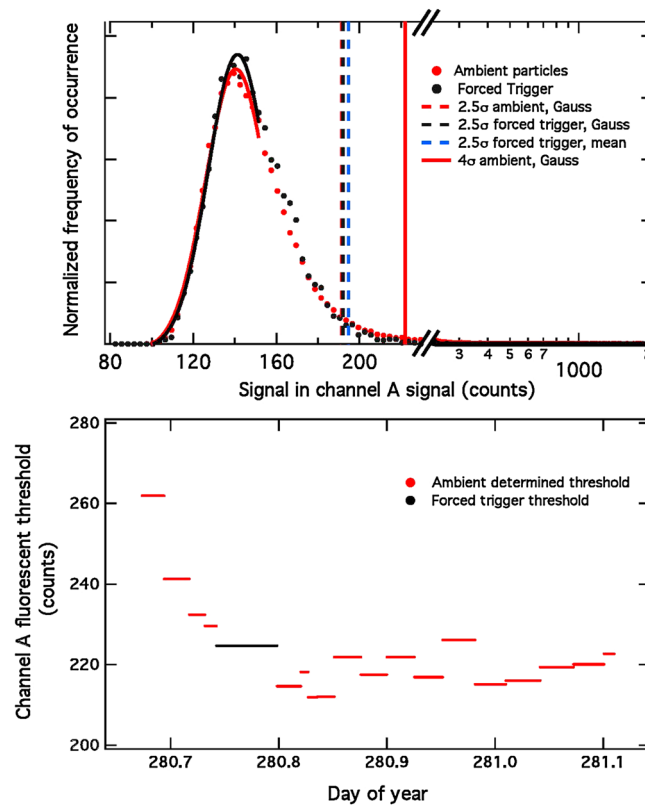
Figure 2. (top) Probability density function of signal recorded in channel A during forced trigger (black) followed directly by normal operation (red) during the flight on 8 October (decimal days 280). Gaussian fits are shown over the range of points used. Fluorescence threshold levels are marked for four different determination strategies as labeled. (bottom) Temporal behavior of fluorescence thresholds determined for channel A over the course of the flight from forced trigger (black) and ambient particles (red).

and background fluorescing material, making the two methods functionally equivalent. Since the fit ignores the histogram tail at high-signal values, this method is expected to be valid even in the presence of ambient biological or other particles exhibiting considerable fluorescence as long as there is a larger underlying population of nonfluorescent particles. Forced trigger mode is still a useful check of the instrument background and stability and, in the case of laboratory studies for which there is no underlying nonfluorescent population, would be the only way to assign an appropriate fluorescence threshold.

Due to the unexplained variability of the background signal in the FL1_280 channel over the course of the project, the threshold above which a particle is considered to be fluorescent is conservatively chosen to be 4 Gaussian widths above the center of the distribution rather than the 2.5 or 3 standard deviation levels used in other studies. The impact of this conservative threshold on observed fluorescent particle concentrations and supermicron fluorescent fractions is discussed in section 3.5 below. The 2.5 and 4 Gaussian widths levels are labeled in Figure 2a for both forced trigger and ambient histograms. Also shown, for comparison to previous work, is the 2.5 standard deviation level determined from the mean and standard deviation of the forced trigger data rather than from the Gaussian fit.

2.1.3. Type Classification

As noted above, the following labels are used here in reference to the three types of fluorescence signals obtained from the WIBS: Channel A refers to signal detected by the FL1 detector (310–400 nm) following excitation at 280 nm, Channel B refers to signal detected by the FL2 detector (420–650 nm) following excitation at 280 nm, and Channel C refers to signal detected by the FL2 detector following excitation at 370 nm. Any given particle can have signal above the fluorescence threshold in one, two, or three of these channels, leading to seven possible combinations of fluorescence signal as shown in Table 1 along with the excitation-emission matrix for the WIBS. From here on we denote particles that exhibit fluorescence above the threshold in only one channel as types A, B, and C; particles that exhibit fluorescence in only two channels are types AB, AC, and BC; and particles that exhibit fluorescence in all three channels are type ABC.

Many previous WIBS studies have not made use of Channel B signals. Some have conservatively identified only particles that exhibit signal in both Channels A and C (which would include our types AC and ABC) to be biological in origin due to known interferences in channel A from nonbiological materials, for example, *Gabey et al.* [2010]. Some studies also interpret the presence of signal in both Channels A and C to be indicative of living biological particles that are still undergoing cellular metabolism, for example, *Toprak and Schnaiter* [2013]. In recent studies in our laboratory, however, we found quite a number of mold spores (metabolically dormant but with a substantial fraction capable of sporulation) that were classified as types A, B, and AB (Figure 3) which would all be missed in an analysis limited to only particles exhibiting signal in both channels

Table 1. The WIBS Excitation-Emission Matrix and the Fluorescent-Type Identities Discussed in the Text[a]

Emission	310–400 nm	420–650 nm
Excitation		
280 nm	Channel A	Channel B
370 nm	Detector Saturated	Channel C

[a]Type A = Signal in channel A only; Type B = signal in channel B only; Type C = signal in channel C only; Type AB = signal in channels A and B; Type AC = signal in channels A and C; Type BC = signal in channels B and C; and Type ABC = signal in channels A, B, and C.

A and C. In addition, in this data set, distinct geographic patterns in concentrations and size distributions were found for the different types classified here; and therefore, there is value in reporting observations of all types. Should there be interest in comparing the present observations with previously published work, the necessary information is fully preserved. For example, the sum of our AC and ABC populations is equivalent to previously reported FL13 categories (also frequently referred to as FBAP).

It is important to note that, while the type classification offers useful information on the fluorescence behavior of the particles sampled, we do not suggest either that the different types are necessarily different particle populations or that a given type always indicates the presence of a certain particle population. For example, in laboratory tests, as shown in Figure 3, it has been observed that certain pure cultures of fungal spores present as a distribution of spectra, which are categorized as a mixture of multiple optical types. To investigate the behavior of known biological materials in the WIBS, pure cultures of fungi were grown on malt extract agar at 20°C and 25% relative humidity until they presented clear spore-bearing physiology. Spores were then aerosolized from sterile glass fungal spore source strength testers using ultrapure nitrogen [*Sivasubramani et al.*, 2004] and introduced, via a stainless steel adapter, into a temperature-controlled chamber from which the WIBS sampled using <1 m of conductive tubing. Here we present these results in Figure 3, which shows the type distributions observed for five different pure spore cultures. It shows that all of these spores have appreciable signal in Channel A while some also have signal in channels B and C. These results are in rough agreement with previous work by *Wlodarski et al.* [2006], which found strong absorption by spores from 200 to 300 nm with emission from 310 to 400 nm and weaker absorption and emission features at longer wavelengths.
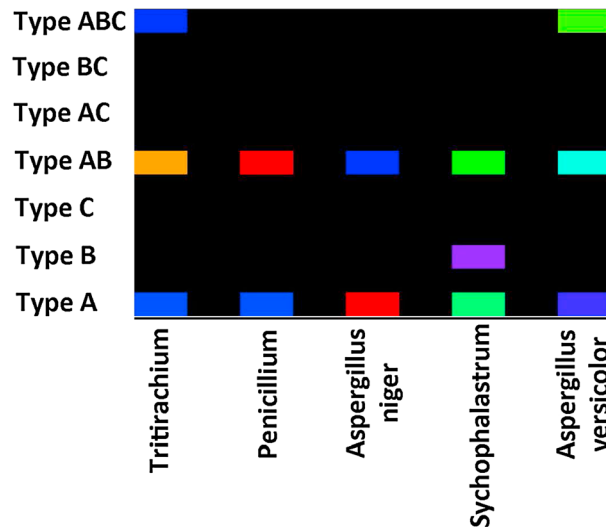
Tritirachium and *Penicillium* both manifest as almost entirely type AB and *Aspergillus niger* manifests as almost entirely type A. In contrast, *Syncephalastrum* manifests as an almost even mixture between types A
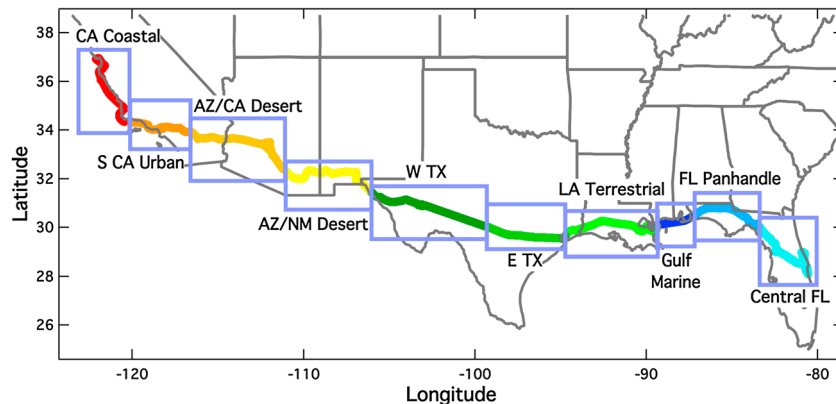

Figure 3. Type manifestations of known fungal spores in the NOAA WIBS during laboratory tests. The colors represent the fraction of that type of spore that appeared in the WIBS as a certain type.

Figure 4. A map of the airship flight path with boxes and coloring indicating the geographic regions discussed in the text.

and AB, and *Aspergillus* versicolor manifests as a mixture of types AB and ABC. In addition, the type classification for a given particle depends not only on the fluorescence behavior of the particle but also on the instrumental gain settings and therefore will vary with instrument setup with different instruments likely giving different classifications. Take, for example, a hypothetical change in the FL2 detector gain while leaving the FL1 detector unchanged. This would not affect the number of particles detected above the threshold in channel A (detected on the unchanged FL1 detector) but could result in an increase in the number of particles detected above the threshold in channels B and C due to a higher sensitivity (i.e., the detection efficiency for weak fluorescence would be increased). Applying this thought experiment to the lab results shown in Figure 3, an increase in the FL2 detector gain could result in conversion of the type A *Syncephalastrum* to type AB or, even, to the appearance of some *Syncephalastrum* as type ABC. Similarly, a decrease in the FL2 detector gain could result in *Syncephalastrum* manifesting as mainly type A with a decrease in the fraction manifesting as type AB. Hence, care should be taken when comparing type distributions detected by different instruments. For a more comprehensive discussion of these issues, please see M. T. Hernandez et al. (manuscript in preparation, 2015).

2.2. Mission Description and Sampling Strategy

The data discussed here were collected during filming of a television documentary called "Operation Cloud Lab: Secrets of the Skies" which was organized and funded by British Broadcasting Corporation (BBC). Details can be found at www.bbc.co.uk/cloudlab. The two-part series aired on BBC 2 in 2014 and focused on improving our understanding of the interactions between biology and weather. The airship, a Skyship 600, began the campaign in Titusville, Florida, on 21 September 2013 and arrived in Monterey, California, on 14 October 2013. Typical operations involved one or two flights on any given flight day with takeoffs in the midmorning (~10 A.M.) and early afternoon (~1 P.M.). The entire study comprised 36 individual flights from coast to coast, 31 of which have been used in this analysis. Most flights occurred over land with one period of extended marine sampling between the Florida panhandle and New Orleans, and some near-coast sampling in California. A map of the flight track is shown in Figure 4. Geographic divisions relevant to later discussion are marked with boxes and variable color. A new "region" was defined during longitudinal travel when either there was a marked shift in either observed PBAP loadings (in the case of the divisions between Central Florida and the Florida panhandle and between east and west Texas) or in geographic features or topography (in the case of all other divisions).

Positional and meteorological data including latitude, longitude, altitude, temperature, and pressure were recorded by an Aircraft-Integrated Meteorological Measurement System (AIMMS-20, Aventech Research, Inc.). There were failures in the AIMMS-20 GPS reception, most notably during sampling over Texas, which led to missing locational data points. For the present analysis, missing data points are interpolated from existing data points to give approximate location information, which is adequate for the level of detail discussed here. In addition to the WIBS, the airship payload included several other particle measurements: a Single-Particle Soot Photometer (SP2) for detection of black carbon; a Photoacoustic Extinctiometer (PAX) for detection of total aerosol light absorption and scattering at 870 nm; and a Cloud Droplet Probe for

measurement of cloud droplet size spectra. The suite of particle measurements, as well as the Aircraft Aerosol Inlet (AAI), was manufactured by Droplet Measurement Technologies, Inc., Boulder, Colorado.

The WIBS was mounted within the airship Gondola in a rack with the PAX, SP2, and gas sampling instruments. The three particle instruments shared the AAI, which was modeled after a passive diffuser inlet used aboard the NASA DC8 by the University of Hawaii, described in detail by *McNaughton et al.* [2007]. Following aspiration into a 0.356 cm inner diameter (i.d.) inlet tip there is an expansion to 1.09 cm i.d. tubing prior to an isokinetic pickoff feeding the WIBS. The WIBS subsamples from the center of the 1.09 cm i.d. line using a pickoff tube with a secondary expansion from 0.25 cm i.d. to 0.47 cm i.d.. After the pickoff, air was delivered to the WIBS through a ~1 m section of conductive tubing with less than 180° of bend and an approximately 10° downward orientation. The volumetric flow into the WIBS was 580 cm^3/min ensuring that the secondary pickoff was isokinetic with the total flow through the inlet of 11 L/min. The total inlet flow was chosen to give an air velocity of 17.5 m/s at the inlet opening so that it would be roughly isokinetic at typical airship speeds between 10 and 20 m/s.

Inlet transmission calculations, assuming spherical particles with density 1 g/cm^3, indicate transmission efficiencies from the ambient to the WIBS detection volume of better than 93% for particles up to 2 μm in diameter decreasing to ~55% at 6 μm and 10% at 10 μm. The majority of the losses occur in the 1 m line from the pickoff to the WIBS, and the effects of variations in airship speed on transmission efficiency are relatively minor. In what follows, the observed concentrations have been adjusted upward as a function of optical size to account for particles lost during sampling. To do this, a size-dependent correction factor was calculated at 1 μm resolution between 1 and 10 μm for the median airship velocity of 17 m/s and normalized size histograms for each type were generated for 2 h blocks of data. The time-dependent correction factor for the concentration of each type (at 2 h resolution) is then the integrated product of the calculated size-dependent correction factor and the normalized observed size histogram. The WIBS also sampled while the airship was on the ground both before and after most flights. These data are later compared to the airborne sampling to assess vertical transport potential of PBAP. A similar upward correction was applied to ground data based on calculated transmission efficiencies when sampling in calm air. The inlet was not optimized for ground sampling, so size-dependent losses are larger than during airborne sampling with transmission efficiencies of better than 87% for particles up to 2 μm, falling to 40% at 6 μm and <5% at 10 μm.

3. Results and Discussion

3.1. Fluorescent Particle Loadings and Size Distributions Aloft

Figure 5 (top) shows observed number concentrations of fluorescent supermicron aerosol above the surface (>100 m) in the 10 geographic regions defined in Figure 4 after correction for inlet transmission efficiency. Error bars show the standard deviation of total fluorescent particle loadings (the sum of all fluorescent types) in each region calculated as the mean of 1 min samples. Figure 5 (middle) shows the percentage contribution of each type to the total supermicron number, and Figure 5 (bottom) shows the fractional contribution of each type to total fluorescent number. In Figure 5 (top to bottom), the different colors (layered consistently top to bottom) represent the contributions of the seven-type classifications to the total. Figure 6 shows the number size distributions of fluorescent particles observed in each region for each type except for type AC, which is omitted because concentrations in all regions were too low to generate statistically significant distributions. For comparison, the total supermicron loadings and number distributions are shown for each region in Figure 7.

The most notable change as the airship moved from east to west was the abrupt shift in both the dominant fluorescent types and in the number distributions observed between east and west Texas. Types AB and ABC, which are the largest components of the total fluorescent load in the east, are lesser contributors in the west where types B, BC, and C are relatively enhanced. There are simultaneous marked shifts to larger sizes for types B, BC, and ABC indicating the presence of different fluorescent PBAP populations that seen in the east. Number distributions for the dominant contributors to the loadings in the Gulf region are shown in Figures 6c and 6f for type AB and ABC, respectively. The solid yellow line shows the distribution observed over the Florida panhandle, solid green line shows that in the Gulf marine boundary layer, and solid red line shows that over Louisiana. In all three regions the median diameter for the type AB signal is ~1.9 μm and that of the type
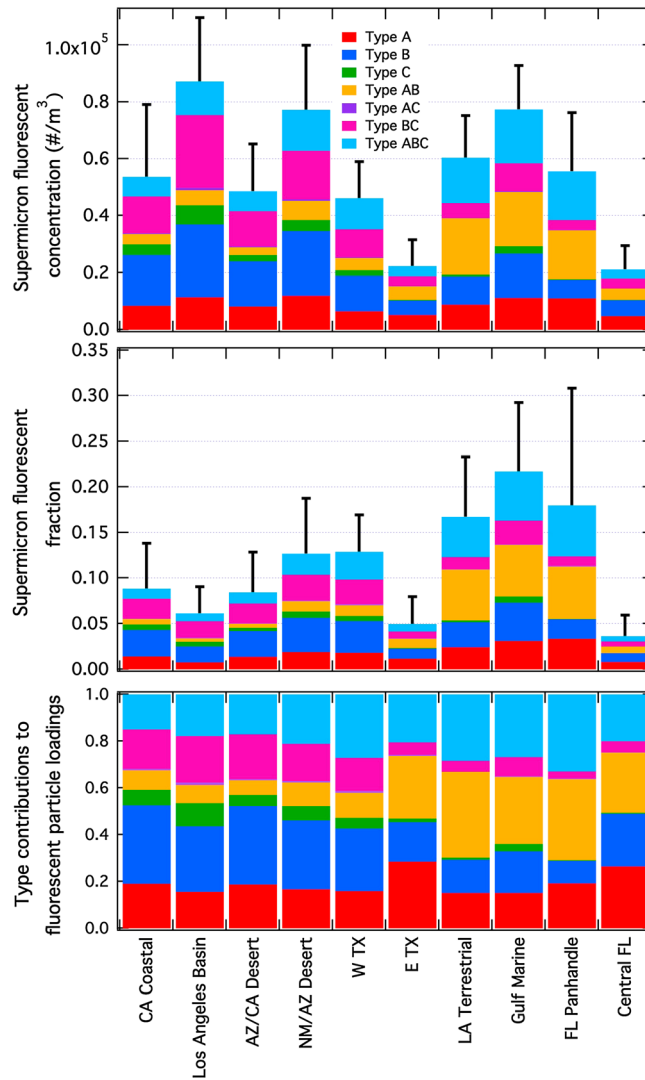
Figure 5. (top) Observed concentrations of fluorescent aerosol in the geographic regions studied are colored by type classification. Error bars show the standard deviation of total fluorescent particle concentrations (the sum of all types) calculated as the means of 1 min samples. (middle) Fractional contribution of fluorescent aerosol to total supermicron particles colored by type classification. Error bars show the standard deviation of total fluorescent supermicron fraction. (bottom) Fractional contribution of each type to observed total fluorescent aerosol loading.

ABC signal is ~2.6 μm. Both types have clear number distributions with median diameters typical of common mold spores in laboratory bioaerosol chamber studies: *Aspergillus* spp., *Penicillium* spp., *Cladosporium* spp., and *Chaetomium* spp.

In contrast, the number distributions for the dominant fluorescent types observed in the west have peaks at larger sizes than are typically observed from laboratory observations of common airborne molds. They are, instead, more representative of the physiology of basidiospores with optical signatures similar to *Agaricus bisporus* spores, which appeared to the WIBS as type ABC with a median diameter of ~6 μm or a variety of pollens several of which appeared as types BC and ABC. Other possible contributors to fluorescent PBAP patterns in the west are pollen fragments, airborne plant debris, or bacteria attached to dust particles. We have aerosolized a selection of dry soil samples in the laboratory and find no fluorescent behavior even for samples with high-organic matter content. This is consistent with previous work [*Pöhlker et al.,* 2012] which found that the fluorescence signature of humic substances was greatly reduced in dry samples relative to wet samples. We therefore do not believe that these signals arise as a result of simple mechanical aerosolization of soil particles containing organic matter.

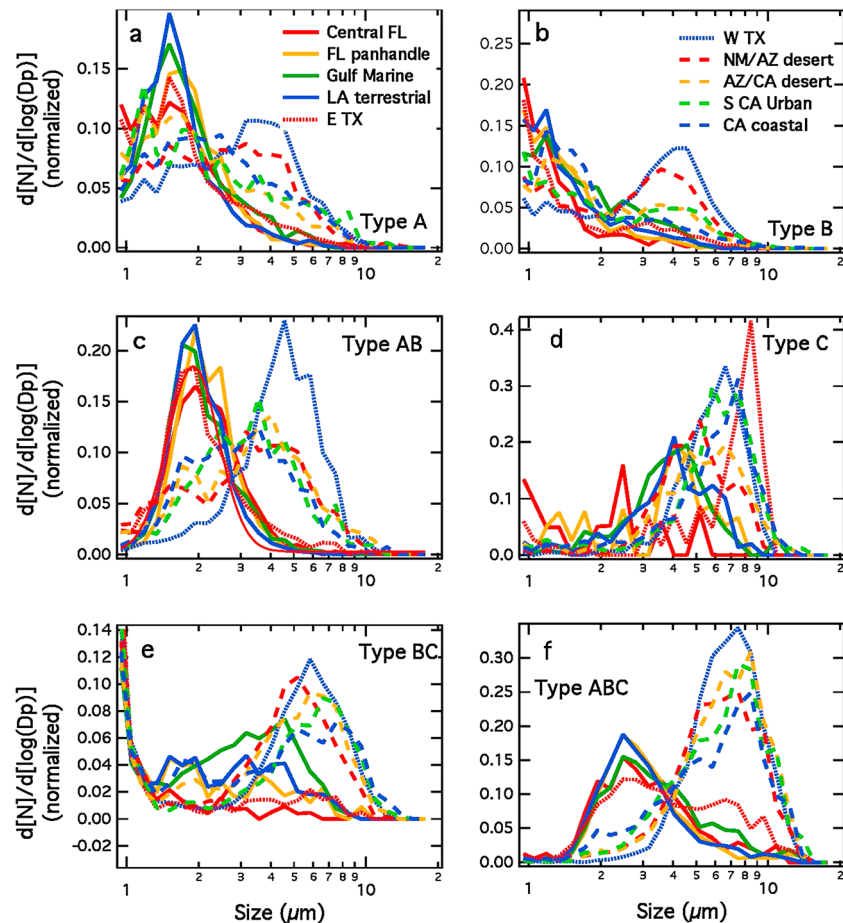These apparently large PBAP may also be present in the east, but they could either be overshadowed by the activity of larger mold spore sources in the region or removed via wet deposition more quickly due to more frequent precipitation events. For comparison, the bulk aerosol supermicron number distributions (Figure 7b) show slight enhancements in particles between 2.5 and 6 μm in the west relative to the east. The fluorescent particle populations are responsible for only a fraction of this enhancement. This may also be a result of less frequent wet removal for supermicron particles and higher-dust emission from dryer soils. Fluorescent particle loadings in the west are nearly as high as those in the east, yet supermicron loadings are higher in the west resulting in smaller fluorescent supermicron fractions there.

Elevated fluorescent particle loadings relative to the surrounding regions were found in the marine boundary layer (MBL) between the Florida panhandle and New Orleans where they were ~$7.7 \pm 1.5 \times 10^4$ m^{-3} on average; this indicates an additional source of PBAP in the Gulf MBL, which is consistent with observations of biomass partitioning from warm marine environments [*Angenent et al.,* 2005; *Blanchard and Syzdek,* 1970; *Paez-Rubio et al.,* 2005]. Loadings in the adjacent over land sampling from the Florida panhandle and

Figure 6. (a–f) Observed number distributions of different fluorescent types in different geographic regions, corrected for inlet transmission efficiency. Type AC is not shown because loadings were never sufficient to produce reasonable number distributions. In Figures 6a–6f the different geographic regions are represented by different line color and patterns as labeled in the legends in Figures 6a and 6b. Types are defined as discussed in the text.

Louisiana were slightly less on average (~6×10^4 m^{-3}), and fluorescent particles accounted for 18–24% by number of total supermicron aerosol in all three areas. The loadings of types A, AB, and ABC are similar between the Florida panhandle, the Gulf MBL, and terrestrial Louisiana. The concentrations in the Gulf MBL are higher than the surrounding terrestrial sampling primarily due to enhanced loadings of types B, C, and BC. Examining the number distributions for these types (solid green lines in Figures 6b, 6d, and 6e), little difference is seen between the Gulf MBL and surrounding terrestrial sampling for types B and C but a distinct size distribution for type BC, peaking at ~4 μm. This could possibly be the signature of a more specific PBAP exhibiting the selection pressures associated with marine sources. The proximity of the coast to the region of the MBL sampled makes it likely that the observations represent a mixture of marine and coastal air.

The Florida panhandle, the Gulf MBL, and terrestrial Louisiana are all very similar in both total PBAP loadings and the dominant types observed. In contrast, central Florida has markedly lower PBAP loadings even though the size distributions observed are generally similar to those seen in the rest of the Gulf region. Several potential causes for this variation were considered. Very recent rain, which was not reported by nearby rain gauges, would lead to removal of large particles, and hence could cause a temporary depression in airborne particle loads, including PBAP. In the case of purely size dependent removal, however, one would expect total supermicron particle concentrations to be reduced and not only fluorescent particles. In fact, the total supermicron particle concentration in central Florida is slightly higher than in the surrounding areas, and the fraction of supermicron particles that are fluorescent is
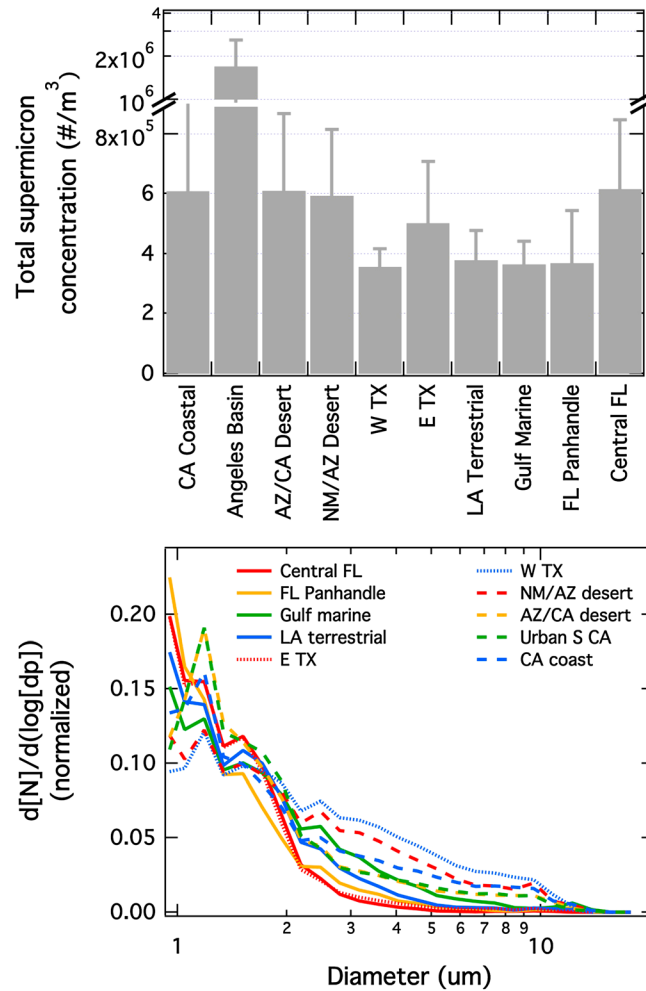
Figure 7. (top) Total supermicron concentrations observed in each geographic region. Note the broken change to log scale on the *y* axis to display loadings observed in the Los Angeles metropolitan area. Error bars show the standard deviation of the mean of 1 min samples. (bottom) Normalized size distributions for all supermicron particles observed in each region.

substantially smaller than in nearby regions, a fraction less than 5% is the lowest observed throughout the mission. Another explanation could be that it was unusually dry in the area, which could decrease emissions of PBAP, especially from fungi. Precipitation gauges in the vicinity of the flight track indicate that around the period of sampling, the area was receiving periodic rain in similar amounts and at similar frequencies to that observed in other regions of the Gulf with higher-fluorescent loadings. The model results (discussed in more detail below) indicate that central Florida is more influenced by clean marine air advecting into the region than are nearby areas.

Another distinct population of fluorescent particles was observed in west Texas. The size distributions for types A, B, and AB observed there are distinct from those observed to either the east or west even though the overall fluorescent loadings are low. All three types (blue dotted lines in Figures 6a–6c) show a peak in number distribution around 4 μm. One likely source of PBAP in the desert of west Texas is livestock production, so these populations may represent emissions from livestock activities in the area. These signals could also represent microbe-dust agglomerates generated from local surface soil. Finally, this region is just north of the Mexican state of Chihuahua, which

has a complex mixture of agricultural and industrial sources and could contribute to distinct fluorescent aerosol signals.

Fluorescent particle loadings observed in the New Mexico/Arizona desert and the Los Angeles basin were the highest observed during the campaign, comparable to loadings observed in the marine boundary layer over the Gulf of Mexico. These observations could be indicative of the presence of large basidiospores, pollen grains (intact or fragments), plant fragments, and/or bacteria attached to dust. The desert between Las Cruces, New Mexico, and Tucson, Arizona, is subject to the North American monsoon and receives most of its rain in August and September although there is no obvious reason for fluorescent aerosol loads to be higher there than in the surrounding areas. The Los Angeles basin is both a large metropolitan area and a region with a significant amount of agriculture and livestock. High-fluorescent particle loadings there could be indicative of either high-bioaerosol loadings or interferences. Note, however, that the size distributions for types C, AB, BC, and ABC in Los Angeles are completely different from the bulk aerosol size distribution, lending credence to the hypothesis that these fluorescent particles are, indeed, PBAP. The size distributions observed for types A and B, which together account for nearly half of the fluorescent particle load in Los Angeles, are more similar to that
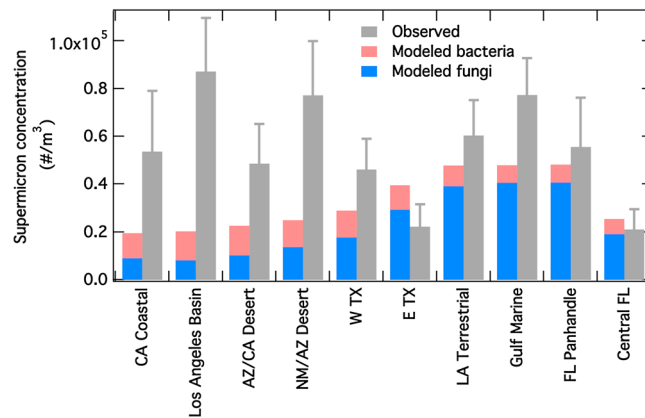
Figure 8. Comparison between observed supermicron fluorescent concentrations and modeled supermicron bacteria and fungi from *Spracklen and Heald* [2014] sampled along the airship coordinates at an altitude of 300 m. Error bars on the observed fluorescent concentrations are determined, as in Figure 5, from the standard deviation of the mean of 1 min samples.

observed for the bulk aerosol yet still seem to have modes at larger sizes. These types may represent a mixture of anthropogenic interferences and PBAP in this region.

3.2. Comparison to Modeled Fungal and Bacterial Loadings

Figure 8 shows a comparison between the observed fluorescent PBAP loadings reported here and modeled concentrations used in the recent *Spracklen and Heald* [2014] study. The model simulation used the GLObal Model of Aerosol Processes (GLOMAP) aerosol [*Mann et al.,* 2010; *Spracklen et al.,* 2005] microphysics scheme within the TOMCAT global 3-D chemical transport model. It was run for the year 2000 and forced by analysis from the European Centre for Medium Range Weather Forecasts. The model has 31 vertical layers between the surface and 10 hPa, and a horizontal resolution of ~2.8° × 2.8°. Note that the model was not run for the year of the observations. The comparison presented here is therefore expected to reflect large-scale regional variations in PBAP sources independent of specific weather events or year-to-year meteorological variability.

The fungal spore emissions scheme implemented in GLOMAP was taken from previous work by *Heald and Spracklen* [2009] where emissions were related to leaf area index and atmospheric water vapor concentrations. The bacterial emissions scheme was based on work by *Hoose et al.* [2010b] and *Burrows et al.* [2009a] where the authors used bacterial loadings reported in the literature to derive ecosystem-dependent bacterial fluxes. Bacteria were assumed to have an emission diameter of 1 μm, and fungal spores were assumed to have a bimodal emission distribution with modes at 1.25 and 6.25 μm. The model was sampled along the airship flight track at an altitude of 300 m during the modeled month matching that in which the airship sampling occurred. For comparison to the data presented here, which are specifically limited to supermicron particles, we have included all of the modeled fungal spores but only the estimated fraction of modeled bacteria (50%) that would fall in the supermicron range.

The model predicts that fungal spores will dominate PBAP loadings in the east, while bacterial emissions will dominate in the west. The model reproduces the observations very well in the east with an average underestimation of 13% in the five eastern regions spanning Central Florida through east Texas. On the other hand, the model predicts only 37% of the observed loadings in the west averaged over the five western regions from west Texas through coastal California. This is consistent with our tentative identification of pollen fragments, plant debris, or bacteria attached to dust as sources for the larger bioaerosol particles in the west, none of which are included in the model. There are reports in the literature [*Lighthart*, 2000; *Tong and Lighthart*, 2000] of observed count median diameters of 3–4 μm for culturable bacteria-containing particles, presumably consisting of bacteria or bacteria-dust agglomerates. If we assumed a larger count median diameter for the modeled bacteria and included all of the modeled bacteria in our comparison rather than only 50%, then the average model underestimate in the east is reduced to less than 1% and that in the west is reduced to approximately a factor of 2. Even assuming all of the modeled bacteria are detectable by the WIBS is inadequate to bring the model and measurements into agreement in the western U.S.

The observed fluorescent particle number distributions in the east are in general agreement with the assumed fungal spore emission diameter, while the observed fluorescent particle number distributions in the west are larger than the prescribed bacterial and fungal diameters in the model. It is also possible that nonbiological fluorescent particle interferences are larger in the west than they are in the east due to either anthropogenic or biomass burning sources. Further work is clearly needed to evaluate the specificity of WIBS fluorescent particle counts in a variety of air masses. As mentioned above, the number distributions of fluorescent particles in

thewest peak at dramatically larger sizes than are seen in the bulk aerosol, in support of our hypothesis that they are biological in origin. While we cannot currently quantify the contribution of any particular biological source to the observed fluorescent populations, the observations presented here show that fluorescent PBAP loadings are considerable in a variety of ecological situations and indicate a need for a better understanding of relationships between fluorescent spectra, PBAP sources, and their transport in the atmosphere.

3.3. Comparisons of Fluorescent PBAP at the Surface and Aloft

The airship spent a limited amount of time in ascent and descent modes so the statistics are poor for any individual vertical profile of number concentrations, and the total number of vertical profiles is small because profiling often only occurred at takeoff and landing. Here we use fluorescent concentration measurements from the ground prior to takeoff and compare them to those observed aloft during flight to extract information about vertical trends in supermicron fluorescent aerosol loadings and populations. To further improve statistics, the ten geographic divisions discussed above have been combined into larger regions; central Florida through eastern Texas have been combined into the "eastern" region and west Texas through coastal California have been combined into the "western" region. As with the number distributions shown in Figure 6, type AC is omitted from the graph because loadings in all regions were too small for the observations to be statistically robust. As discussed in section 2.2 above, size-dependent upward corrections have been applied to both airborne and ground-based data based on calculated inlet transmission efficiencies.

Care must be taken when comparing surface data collected at airfields (which may not be representative of local conditions) and flight data collected between airfields (in possibly more remote regions). There are several reasons that such a comparison is likely valid in the present study. First, the airship, due to its slow airspeed and docking requirements, typically used small rural airfields far from major transport hubs. Thus, a comparison between surface observations and flight data is likely more valid for this project than for many other airborne projects where runway data are heavily impacted by local aircraft and urban emissions. Second, the airship typically made two short (~2 h) flights per day with a stop to refuel in between. The first takeoff was usually around 10 A.M. and the second was usually in the early afternoon so that, in any given day, multiple short flights are bracketed by ground sampling at different times of day, negating the likelihood of a strong bias in the average ground data due to diurnal boundary layer variations. Finally, with only one exception, for all fluorescent types and in all regions, observed size distributions were independent of altitude. The exception is for type A particles and is discussed in more detail below. A similar consistency is seen between the contribution of each type to total fluorescent particle loadings at the surface and aloft. These comparisons indicate that sampling at the ground and aloft is representative of regional fluorescent particle distributions and thus PBAP. In what follows we examine the relationship between loadings observed at the surface and aloft in order to build a basic understanding of the vertical transport of fluorescent PBAP.

Figure 9a (bottom) shows the concentrations of each type of fluorescent aerosol at the surface and aloft. Figure 9a (top) shows the ratio of the concentration aloft to that at the surface. Excepting type A particles, in the east the concentration aloft for all fluorescent types is ~25–55% of the surface concentration, while in the west the concentration aloft is 5–15% of that at the surface. Figure 9b (bottom) shows the fraction of supermicron particles exhibiting a given type of fluorescence signature at the surface and aloft in the east and west. Figure 9b (top) shows the ratio of the fluorescent fraction aloft to that at the surface. In the east, for all types other than type A, the fluorescent fraction aloft is similar to that observed at the surface indicating that the upward transport of PBAP is similar to that of total supermicron aerosol. The ratio of the fluorescent fraction aloft to that at the surface is lower in the west than in the east (Figure 9b, top), also consistent with purely size dependent vertical transport since the dominant fluorescent types have modes at larger sizes in the west than in the east. As shown in Figure 7, the total aerosol number distributions observed by the WIBS in both the east and the west are similar and continue to increase below the detection limit of the WIBS, so if upward transport was simply a function of particle size we would expect to find reduced supermicron fluorescent fractions aloft associated with larger diameter PBAP sources.

3.4. Potential Anthropogenic Interference in Type A Particles

As noted above, comparisons at the surface and aloft for type A particles were anomalous as compared to the other fluorescent particle types. First, these particles at the surface in both regions were markedly smaller
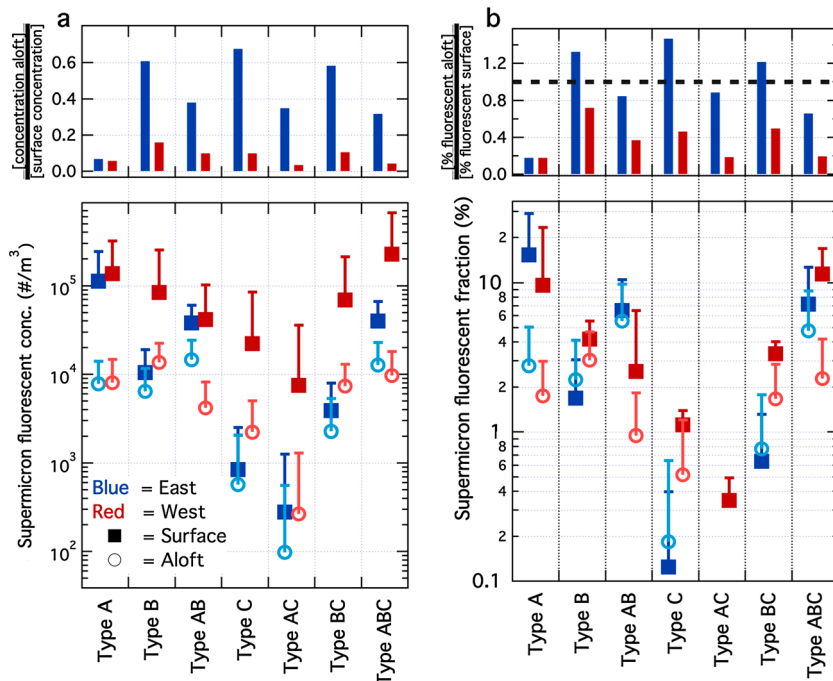
Figure 9. (a) Supermicron fluorescent particle concentrations by type at the surface (filled squares) and aloft (open circles, corrected to STP) in the east (blue) and west (red). Figure 9a (top) shows the ratio of the concentration at STP observed aloft to that observed at the surface. (b) Percentage of supermicron particles exhibiting fluorescence of each type at the surface (filled squares) and aloft (open circles). Figure 9b (top) shows the ratio of the fraction observed aloft to that observed at the surface.

than aloft. At the surface the number size distributions did not have an identifiable peak within the detection range of the WIBS. Aloft the sizes peaked between 1 and 2 μm in the east and between 2 and 3 μm in the west. Second, the concentrations of type A particles at the surface were relatively high and represented a much larger fraction of total supermicron concentrations than they did aloft. An observation of high concentrations of smaller particles at the surface likely indicates a proximity to a source that is not representative of the regional background.

Work by *Pöhlker et al.* [2012] shows that naphthalene would appear as "type A" to the WIBS since it absorbs at around 280 nm and emits between 300 and 400 nm. We therefore hypothesize that high concentrations of type A at the surface are due to the presence of an anthropogenic interferent such as naphthalene or a spectrally similar compounds (e.g., polycyclic aromatic hydrocarbon). It is possible that anthropogenic interferents are also affecting reported type A fluorescent particle concentrations aloft. *Toprak and Schnaiter* [2013] found ~0.2% of black carbon particles and 10% of dust particles would fluoresce in the FL1 channel, although they noted that the high fraction of fluorescent dust particles could be the result of bacteria on dust. A general correspondence during flight was observed between spikes in WIBS type A particles and spikes in refractory black carbon as measured by the SP2, likely the result of aromatic compounds being associated with BC particles rather than fluorescence from the BC itself. As also reported by Toprak and Schnaiter, however, bacteria (specifically *Pseudomonas syringae*) manifest in the WIBS as type A. Therefore, the particles observed with this signature in the atmosphere are almost certainly a mixture of fluorescent biological particles and nonbiological fluorescent interferences. Unfortunately, it is currently impossible to determine the relative magnitudes of these two components of the type A signal; however, the airborne type A number distributions are distinct from the bulk aerosol size distributions, with modes at larger sizes, likely indicating a dominance of biological particles in this channel during airborne sampling. Similarly, we find no evidence for contamination from nonbiological sources in any spectral assignment, other than type A for this particular data set.

3.5. Effects of Trigger Level on Reported Loadings

Here we have used a more conservative fluorescence threshold level (4 Gaussian widths) than previous studies to account for the fact that our signal baseline was more variable than previously observed. If, instead,

the previously reported 2.5 Gaussian widths level was used as the fluorescence threshold, we would report higher-fluorescent particle loadings by a moderate margin (~40%) in the Gulf region and a large margin (~80%) in the west. Type A particles stand out as anomalous with very large increases in loading calculated with the lower trigger threshold, especially in urban areas. Type A loadings near Houston increase by a factor of 3 and those in urban southern California by a factor of 4.8 using a 2.5 Gaussian widths level threshold relative to a 4 Gaussian widths level. It is possible that the nonbiological anthropogenic contaminants that manifest as type A are more weakly fluorescent than fluorescent biological particles leading to an increased sensitivity of type A classification to fluorescence threshold in the present study. Other than these significant changes to the fraction of particles exhibiting type A fluorescence, our choice of trigger level has no appreciable impact on the relative importance of the different types in the different regions or on the observed number distributions. Clearly, there is a need for improved understanding of the impacts of instrument gain, chosen trigger levels, and nonbiological fluorescent interferents on reported PBAP loadings. In the present study, despite apparent potential for anthropogenic interference in the type A signal, we find it likely that the total fluorescent particle loadings reported here underestimate the actual fluorescent PBAP loadings in the atmosphere. As discussed above, it is likely that a fraction of the type A fluorescent particles are biological in origin, especially in the airborne data. Even if the entirety of the type A signal was due to fluorescent anthropogenic interferents, the total fluorescent PBAP concentrations reported here are likely lower limits due to our conservative fluorescence threshold determination.

4. Conclusions

Here we have reported the first airborne measurements of fluorescent particle loading observations, which are associated with PBAP concentrations and characteristics, made using a WIBS instrument. The measurements cover a wide range of longitude over the continental U.S. and provide constraints for models simulating PBAP concentrations in a diverse range of environments. A new method was presented for analyzing WIBS data by segregating fluorescent aerosol into seven types based on their fluorescence behavior in each of the three WIBS channels. This yields information on fluorescent aerosol populations that can, in certain situations, allow for approximate attribution of different populations to various biological sources and anthropogenic interferents. We find appreciable loadings in the Gulf region (up to $7.7 \pm 1.5 \times 10^4\,\mathrm{m}^{-3}$) and in the arid west (up to $8.7 \pm 2.2 \times 10^4\,\mathrm{m}^{-3}$) with significant differences in the kind of fluorescent aerosol observed between the two regions. Much of the fluorescent aerosol in the Gulf region is found to be between 1 and 4 μm in diameter, similar in size and type classification to common mold spores aerosolized in laboratory chambers, whereas much of that in the west is found at larger sizes (3–10 μm) possibly attributable to basidiospores, fragments of pollen, plant debris, and/or bacteria attached to dust. Fluorescent PBAP accounted for 3–24% of total supermicron particles in the east and 5 to 12% in the western U.S. A comparison of the present observations with modeled PBAP loadings shows good agreement in the southeastern U.S. and a moderate underestimate by the model (a factor of ~2.7 on average) in the southwestern U.S. The prescribed PBAP sizes in the model are in reasonable agreement with observations in the east while they are smaller than observed in the west. This analysis indicates that PBAP can be present in high concentrations and represent a significant fraction of supermicron particles even in arid environments and highlights the need for further observations of PBAP in a variety of ecosystems and in the free troposphere. Furthermore, our analysis of particle type suggests that there may be important sources of supermicron bioaerosol (e.g., pollen fragments and plant debris) particularly in the western U.S., which are neglected in the model. Comparison of loadings observed at the surface and aloft indicates that fluorescent PBAP is transported upward with similar efficiency to other supermicron aerosol, indicating that they are likely to make up a similar fraction of supermicron aerosol in the free troposphere to the fluorescent fraction in the boundary layer.

References

Angenent, L. T., S. T. Kelley, A. St Amand, N. R. Pace, and M. T. Hernandez (2005), Molecular identification of potential pathogens in water and air of a hospital therapy pool, *Proc. Natl. Acad. Sci. U.S.A.*, *102*(13), 4860–4865.

Blanchard, C., and L. Syzdek (1970), Mechanism for water-to-air transfer and concentration of bacteria, *Science*, *170*(3958), 626–628.

Bowers, R. M., C. L. Lauber, C. Wiedinmyer, M. Hamady, A. G. Hallar, R. Fall, R. Knight, and N. Fierer (2009), Characterization of airborne microbial communities at a high-elevation site and their potential to act as atmospheric ice nuclei, *Appl. Environ. Microbiol.*, *75*(15), 5121–5130.

Bowers, R. M., I. B. McCubbin, A. G. Hallar, and N. Fierer (2012), Seasonal variability in airborne bacterial communities at a high-elevation site, *Atmos. Environ.*, *50*, 41–49.

Burrows, S. M., W. Elbert, M. G. Lawrence, and U. Pöschl (2009a), Bacteria in the global atmosphere—Part 1: Review and synthesis of literature data for different ecosystems, *Atmos. Chem. Phys.*, *9*(23), 9263–9280.

Burrows, S. M., T. Butler, P. Jöckel, H. Tost, A. Kerkweg, U. Pöschl, and M. G. Lawrence (2009b), Bacteria in the global atmosphere—Part 2: Modeling of emissions and transport between different ecosystems, *Atmos. Chem. Phys.*, *9*(23), 9281–9297.

Burrows, S. M., C. Hoose, U. Pöschl, and M. G. Lawrence (2013), Ice nuclei in marine air: Biogenic particles or dust?, *Atmos. Chem. Phys.*, *13*(1), 245–267.

Christner, B. C., C. E. Morris, C. M. Foreman, R. M. Cai, and D. C. Sands (2008), Ubiquity of biological ice nucleators in snowfall, *Science*, *319*(5867), 1214–1214.

Crawford, I., et al. (2012), Ice formation and development in aged, wintertime cumulus over the UK: Observations and modelling, *Atmos. Chem. Phys.*, *12*(11), 4963–4985.

Creamean, J. M., et al. (2013), Dust and biological aerosols from the Sahara and Asia influence precipitation in the western U.S., *Science*, *339*(6127), 1572–1578.

DeLeon-Rodriguez, N., T. L. Lathem, L. M. Rodriguez-R, J. M. Barazesh, B. E. Anderson, A. J. Beyersdorf, L. D. Ziemba, M. Bergin, A. Nenes, and K. T. Konstantinidis (2013), Microbiome of the upper troposphere: Species composition and prevalence, effects of tropical storms, and atmospheric implications, *Proc. Natl. Acad. Sci. U.S.A.*, *110*(7), 2575–2580.

Delort, A.-M., M. Vaitilingom, P. Amato, M. Sancelme, M. Parazols, G. Mailhot, P. Laj, and L. Deguillaume (2010), A short overview of the microbial population in clouds: Potential roles in atmospheric chemistry and nucleation processes, *Atmos. Res.*, *98*(2–4), 249–260.

Després, V. R., et al. (2012), Primary biological aerosol particles in the atmosphere: A review, *Tellus, Ser. B, 64*, 15598, doi:10.3402/tellusb.v64i0.15598.

Diehl, K., S. Matthias-Maser, R. Jaenicke, and S. K. Mitra (2002), The ice nucleating ability of pollen: Part II. Laboratory studies in immersion and contact freezing modes, *Atmos. Res.*, *61*(2), 125–133.

Gabey, A. M., M. W. Gallagher, J. Whitehead, J. R. Dorsey, P. H. Kaye, and W. R. Stanley (2010), Measurements and comparison of primary biological aerosol above and below a tropical forest canopy using a dual channel fluorescence spectrometer, *Atmos. Chem. Phys.*, *10*(10), 4453–4466.

Gabey, A. M., M. Vaitilingom, E. Freney, J. Boulon, K. Sellegri, M. W. Gallagher, I. P. Crawford, N. H. Robinson, W. R. Stanley, and P. H. Kaye (2013), Observations of fluorescent and biological aerosol at a high-altitude site in central France, *Atmos. Chem. Phys.*, *13*(15), 7415–7428.

Hallar, A. G., G. Chirokova, I. McCubbin, T. H. Painter, C. Wiedinmyer, and C. Dodson (2011), Atmospheric bioaerosols transported via dust storms in the western United States, *Geophys. Res. Lett.*, *38*, L17801, doi:10.1029/2011GL048166.

Heald, C. L., and D. V. Spracklen (2009), Atmospheric budget of primary biological aerosol particles from fungal spores, *Geophys. Res. Lett.*, *36*, L09806, doi:10.1029/2009GL037493.

Healy, D. A., D. J. O'Connor, and J. R. Sodeau (2012a), Measurement of the particle counting efficiency of the "Waveband Integrated Bioaerosol Sensor" model number 4 (WIBS-4), *J. Aerosol Sci.*, *47*, 94–99.

Healy, D. A., D. J. O'Connor, A. M. Burke, and J. R. Sodeau (2012b), A laboratory assessment of the Waveband Integrated Bioaerosol Sensor (WIBS-4) using individual samples of pollen and fungal spore material, *Atmos. Environ.*, *60*, 534–543.

Healy, D. A., J. A. Huffman, D. J. O'Connor, C. Pöhlker, U. Pöschl, and J. R. Sodeau (2014), Ambient measurements of biological aerosol particles near Killarney, Ireland: A comparison between real-time fluorescence and microscopy techniques, *Atmos. Chem. Phys.*, *14*, 8055–8069, doi:10.5194/acp-14-8055-2014.

Hill, S. C., R. G. Pinnick, S. Niles, N. F. Fell, Y. L. Pan, J. Bottiger, B. V. Bronk, S. Holler, and R. K. Chang (2001), Fluorescence from airborne microparticles: Dependence on size, concentration of fluorophores, and illumination intensity, *Appl. Opt.*, *40*(18), 3005–3013.

Hill, S. C., M. W. Mayo, and R. K. Chang (2009), *Fluorescence of Bacteria, Pollens and Naturally Occurring Airborne Particles: Excitation/Emission Spectra*, ARL-TR-4722, Army Res. Lab., Adelphi, Md.

Hill, T. C. J., B. F. Moffett, P. J. DeMott, D. G. Georgakopoulos, W. L. Stump, and G. D. Franc (2014), Measurement of ice nucleation-active bacteria on plants and in precipitation by quantitative PCR, *Appl. Environ. Microbiol.*, *80*(4), 1256–1267.

Hoose, C., J. E. Kristjánsson, and S. M. Burrows (2010a), How important is biological ice nucleation in clouds on a global scale?, *Environ. Res. Lett.*, *5*(2), doi:10.1088/1748-9326/5/2/024009.

Hoose, C., J. E. Kristjánsson, J.-P. Chen, and A. Hazra (2010b), A classical-theory-based parameterization of heterogeneous ice nucleation by mineral dust, soot, and biological particles in a global climate model, *J. Atmos. Sci.*, *67*(8), 2483–2503.

Huffman, J. A., B. Treutlein, and U. Pöschl (2010), Fluorescent biological aerosol particle concentrations and size distributions measured with an Ultraviolet Aerodynamic Particle Sizer (UV-APS) in Central Europe, *Atmos. Chem. Phys.*, *10*(7), 3215–3233.

Huffman, J. A., B. Sinha, R. M. Garland, A. Snee-Pollmann, S. S. Gunthe, P. Artaxo, S. T. Martin, M. O. Andreae, and U. Pöschl (2012), Size distributions and temporal variations of biological aerosol particles in the Amazon rainforest characterized by microscopy and real-time UV-APS fluorescence techniques during AMAZE-08, *Atmos. Chem. Phys.*, *12*(24), 11,997–12,019.

Iannone, R., D. I. Chernoff, A. Pringle, S. T. Martin, and A. K. Bertram (2011), The ice nucleation ability of one of the most abundant types of fungal spores found in the atmosphere, *Atmos. Chem. Phys.*, *11*(3), 1191–1201.

Jacobson, M. Z., and D. G. Streets (2009), Influence of future anthropogenic emissions on climate, natural emissions, and air quality, *J. Geophys. Res.*, *114*, D08118, doi:10.1029/2008JD011476.

Jaenicke, R., S. Matthias-Maser, and S. Gruber (2007), Omnipresence of biological material in the atmosphere, *Environ. Chem.*, *4*(4), 217–220.

Joly, M., E. Attard, M. Sancelme, L. Deguillaume, C. Guilbaud, C. E. Morris, P. Amato, and A. M. Delort (2013), Ice nucleation activity of bacteria isolated from cloud water, *Atmos. Environ.*, *70*, 392–400.

Kaye, P. H., W. R. Stanley, E. Hirst, E. V. Foot, K. L. Baxter, and S. J. Barrington (2005), Single particle multichannel bio-aerosol fluorescence sensor, *Opt. Express*, *13*(10), 3583–3593.

Konwar, M., R. S. Maheskumar, J. R. Kulkarni, E. Freud, B. N. Goswami, and D. Rosenfeld (2012), Aerosol control on depth of warm rain in convective clouds, *J. Geophys. Res.*, *117*, D13204, doi:10.1029/2012JD017585.

Lighthart, B. (2000), Mini-review of the concentration variations found in the alfresco atmospheric bacterial populations, *Aerobiologia*, *16*(1), 7–16.

Mann, G. W., K. S. Carslaw, D. V. Spracklen, D. A. Ridley, P. T. Manktelow, M. P. Chipperfield, S. J. Pickering, and C. E. Johnson (2010), Description and evaluation of GLOMAP-mode: A modal global aerosol microphysics model for the UKCA composition-climate model, *Geosci. Model Dev.*, *3*(2), 519–551.

McNaughton, C. S., et al. (2007), Results from the DC-8 Inlet Characterization Experiment (DICE): Airborne versus surface sampling of mineral dust and sea salt aerosols, *Aerosol Sci. Technol.*, *41*(2), 136–159.

Morris, C. E., F. Conen, J. A. Huffman, V. Phillips, U. Pöschl, and D. C. Sands (2014), Bioprecipitation: A feedback cycle linking Earth history, ecosystem dynamics and land use through biological ice nucleators in the atmosphere, *Global Change Biol.*, *20*(2), 341–351.

O'Connor, D. J., D. A. Healy, S. Hellebust, J. T. M. Buters, and J. R. Sodeau (2014), Using the WIBS-4 (Waveband Integrated Bioaerosol Sensor) technique for the on-line detection of pollen grains, *Aerosol Sci. Technol.*, *48*(4), 341–349.

Paez-Rubio, T., E. Viau, S. Romero-Hernandez, and J. Peccia (2005), Source bioaerosol concentration and rRNA gene-based identification of microorganisms aerosolized at a flood irrigation wastewater reuse site, *Appl. Environ. Microbiol.*, *71*(2), 804–810.

Pan, Y. L., J. L. Santarpia, S. Ratnesar-Shumate, E. Corson, J. Eshbaugh, S. C. Hill, C. C. Williamson, M. Coleman, C. Bare, and S. Kinahan (2014a), Effects of ozone and relative humidity on fluorescence spectra of octapeptide bioaerosol particles, *J. Quant. Spectrosc. Radiat. Transfer*, *133*, 538–550.

Pan, Y. L., et al. (2014b), Spectrally-resolved fluorescence cross sections of aerosolized biological live agents and simulants using five excitation wavelengths in a BSL-3 laboratory, *Opt. Express*, *22*(7), 8165–8189.

Pöhlker, C., J. A. Huffman, and U. Pöschl (2012), Autofluorescence of atmospheric bioaerosols—Fluorescent biomolecules and potential interferences, *Atmos. Meas. Tech.*, *5*(1), 37–71.

Pöschl, U., et al. (2010), Rainforest Aerosols as biogenic nuclei of clouds and precipitation in the Amazon, *Science*, *329*(5998), 1513–1516.

Pratt, K. A., P. J. DeMott, J. R. French, Z. Wang, D. L. Westphal, A. J. Heymsfield, C. H. Twohy, A. J. Prenni, and K. A. Prather (2009), In situ detection of biological particles in cloud ice-crystals, *Nat. Geosci.*, *2*(6), 397–400.

Sesartic, A., and T. N. Dallafior (2011), Global fungal spore emissions, review and synthesis of literature data, *Biogeosciences*, *8*(5), 1181–1192.

Sesartic, A., U. Lohmann, and T. Storelvmo (2013), Modelling the impact of fungal spore ice nuclei on clouds and precipitation, *Environ. Res. Lett.*, *8*(1), doi:10.1088/1748-9326/8/1/014029.

Sivasubramani, S. K., R. T. Niemeier, T. Reponen, and S. A. Grinshpun (2004), Fungal spore source strength tester: Laboratory evaluation of a new concept, *Sci. Total Environ.*, *329*(1–3), 75–86.

Smith, D. J., H. J. Timonen, D. A. Jaffe, D. W. Griffin, M. N. Birmele, K. D. Perry, P. D. Ward, and M. S. Roberts (2013), Intercontinental dispersal of bacteria and archaea by transpacific winds, *Appl. Environ. Microbiol.*, *79*(4), 1134–1139.

Spracklen, D. V., and C. L. Heald (2014), The contribution of fungal spores and bacteria to regional and global aerosol number and ice nucleation immersion freezing rates, *Atmos. Chem. Phys.*, *14*, 9051–9059, doi:10.5194/acp-14-9051-2014.

Spracklen, D. V., K. J. Pringle, K. S. Carslaw, M. P. Chipperfield, and G. W. Mann (2005), A global off-line model of size-resolved aerosol microphysics: I. Model development and prediction of aerosol properties, *Atmos. Chem. Phys.*, *5*, 2227–2252.

Tong, Y. Y., and B. Lighthart (2000), The annual bacterial particle concentration and size distribution in the ambient atmosphere in a rural area of the Willamette valley, Oregon, *Aerosol Sci. Technol.*, *32*(5), 393–403.

Toprak, E., and M. Schnaiter (2013), Fluorescent biological aerosol particles measured with the Waveband Integrated Bioaerosol Sensor WIBS-4: Laboratory tests combined with a one year field study, *Atmos. Chem. Phys.*, *13*(1), 225–243.

Wlodarski, M., M. Kaliszewski, M. Kwasny, K. Kopczynski, Z. Zawadzki, Z. Mierczyk, J. Mlynczak, E. Trafny, and M. Szpakowska (2006), Fluorescence excitation-emission matrices of selected biological materials, in *Optically Based Biological and Chemical Detection for Defence III*, edited by J. C. Carrano and A. Zukauskas, Stockholm.